DOI: 10.1590/2317-4889201720170064

ARTICLE

Zircon U-Pb geochronology, Sm-Nd and Pb-Pb isotope systematics of Ediacaran post-collisional high-silica Acampamento Velho volcanism at the Tupanci area, NW of the Sul-Rio-Grandense Shield, Brazil

Geocronologia U-Pb em zircão e isótopos Sm-Nd e Pb-Pb no vulcanismo Ediacarano alta-sílica da Formação Acampamento Velho na região do Tupanci, NW do Escudo Sul-Rio-Grandense, Brasil

Carlos Augusto Sommer[1], Felipe Padilha Leitzke[1,2]*, Evandro Fernandes de Lima[1], Carla Joana Santos Barreto[1,6], Jean Michel Lafon[5], Vinicius Matté[1,3], Ruy Paulo Philipp[1], Rommulo Vieira Conceição[1], Miguel Ângelo Stipp Basei[4]

ABSTRACT: We present new U-Pb zircon ages and Sm-Nd-Pb isotopic data for volcanic and hypabyssal acid rocks from the northernmost exposure of the Acampamento Velho Formation in the NW portion of the Sul-Rio-Grandense Shield, Brazil. The first volcanic episode, grouped in the high-Ti rhyolites from the Tupanci hill, shows age of 579 ± 5.6 Ma, which is in agreement with the post-collisional Acampamento Velho Formation volcanism in the Bom Jardim Group of the Camaquã Basin. A poorly constrained age of 558 +/- 39 Ma was obtained for rhyolites from the low-Ti group at the Picados Hill, which may indicate a younger acid volcanism, or a greater time span for the volcanism of the Acampamento Velho Formation in southernmost Brazil. Regarding magmatic sources, Sm/Nd isotopic data coupled to Pb isotopes and a review of trace element geochemistry indicate different amounts of Paleoproterozoic (Dom Feliciano, Pinheiro Machado Suite) to Neoproterozoic (Rio Vacacaí terrane) lower crust melting. Our data, coupled with literature data, contribute to a better understanding of the stratigraphic evolution for the Neoproterozoic post-collisional volcanic successions of the Camaquã Basin in the Sul-Rio-Grandense Shield.

KEYWORDS: Volcanism; Acampamento Velho Formation; Camaquã Basin; Tupanci; Geochronology.

RESUMO: *Novas idades obtidas por meio do método U-Pb em zircão e dados isotópicos Sm-Nd-Pb são apresentados para as rochas vulcânicas e hipabssais ácidas da exposição mais setentrional da Formação Acampamento Velho na porção NW do Escudo Sul-Rio-Grandense, Brasil. O primeiro episódio vulcânico, agrupado nos riolitos alto-Ti do Cerro Tupanci, possui idades de 579 ± 5,6 Ma, o que está de acordo com dados da literatura para o vulcanismo pós-colisional da Formação Acampamento Velho na Bacia do Camaquã. Idades de 558 +/- 39 Ma foram obtidas para o grupo de riolitos baixo-Ti no Cerro dos Picados, o que pode indicar um episódio vulcânico mais recente ou um período de tempo maior para o vulcanismo da Formação Acampamento Velho no Sul do Brasil, embora o grau de incerteza nos dados seja alto. Em relação às fontes magmáticas, os dados isotópicos de Sm-Nd acoplados a isótopos de Pb e uma revisão da geoquímica de elementos-traço indicam diferentes graus de fusão de crosta inferior paleoproterozoica (Suíte Dom Feliciano, Pinheiro Machado) a neoproterozoica (Terreno Rio Vacacaí). Os dados apresentados neste estudo, quando analisados em conjunto com dados da literatura, contribuem para a melhor compreensão da evolução estratigráfica das sucessões vulcânicas neoproterozoicas pós-colisionais da Bacia do Camaquã no Escudo Sul-Rio-Grandense.*

PALAVRAS-CHAVE: *Vulcanismo; Formação Acampamento Velho; Bacia do Camaquã; Tupanci; Geocronologia.*

[1]Instituto de Geociências, Universidade Federal do Rio Grande do Sul – UFRGS, Porto Alegre (RS), Brazil. *E-mails: casommer@sinos.net, eflgeologo@gmail.com, ruy.philipp@ufrgs.br, rommulo.conceicao@ufrgs.br*

[2]Steinmann Institut für Geologie, Mineralogie and Paläontologie, Universität Bonn. *E-mail: felipeplgeo@gmail.com*

[3]Universidade Federal do Pampa – UNIPAMPA, Bagé (RS), Brazil. *E-mail:vinimatte@msn.com*

[4]CPGeo/IGc/Universidade de São Paulo – USP, São Paulo (SP), Brazil. *E-mail:baseimas@usp.br*

[5]Laboratório de Geologia Isotópica, Universidade Federal do Pará – UFPA, Belém (PA), Brazil. *E-mail:lafonjm@ufpa.br*

[6]Centro de Tecnologia e Geociências, Universidade Federal de Pernambuco – UFPE, Recife (PE), Brazil. *E-mail:carlabarreto.geo@hotmail.com*

*Corresponding author.

Manuscript ID: 20170064. **Received in:** 05/03/2017. **Approved in:** 09/29/2017.

INTRODUCTION

The Sul-Rio-Grandense Shield (SRGS) in southernmost Brazil is constituted by rocks related to the Brasiliano/Pan-African orogenic cycle emplaced in a Paleoproterozoic metamorphic basement (Hartmann *et al.* 1999, Soliani *et al.* 2000, Nardi *et al.* 2008). The magmatism in this era was developed in two main phases: arc-related environment, with ages from 850–700 Ma; and post-collisional environment (Liégeois 1998), with ages from 650–535 Ma, marked by magmatism along transcurrent shear zones (Fernandes *et al.* 1995, Babinski *et al.* 1997, Bitencourt & Nardi 2000, Chemale Jr. 2000, Hartmann *et al.* 2000, 2007, Nardi & Bitencourt 2009).

The post-collisional stage in the eastern portion of the SRGS is marked by a shear belt with voluminous granitic magmatism in the Pelotas Batholith (Philipp *et al.* 2000). General aspects of this extensive granite production episode in the Pelotas Batholith include syn-transcurrent, high-K, calc-alkaline and peraluminous granites that evolve to shoshonitic affinity and late to post-transcurrent, dominantly metaluminous alkaline granites (Philipp & Machado 2005). Excluding the leucocratic peraluminous granites, all granitoid types have basic magmatic rocks associated, normally represented by mafic microgranular enclaves and dykes in commingling systems (Bitencourt & Nardi 2000). Western and northwestern portions of the SRGS represent less deformed areas, with volcano-sedimentary sequences associated with the Camaquã Basin (Fig. 1). Magmatism in the W and NW portion of the SRGS developed mainly between 650–530 Ma and shares a similar geochemical evolution as observed in the eastern part of the SRGS, with the presence of high-K, calc-alkaline granitoids, shoshonitic and tholeitic pluto-no-volcanic sequences (Nardi *et al.* 2008). The sedimentary sequences in the Camaquã Basin evolve from shallow marine in the Maricá Formation to lacustrine and alluvial in the Bom Jardim and Camaquã groups (Paim *et al.* 2000).

Magmatism in the Bom Jardim Group is related to the Lavras do Sul Shoshonitic Association, which is plutonic and volcanic basic to acid rocks mainly with ages between 610–590 Ma (Lima & Nardi 1985). Volcanism in the Bom Jardim Group (Fig. 1) was established predominantly

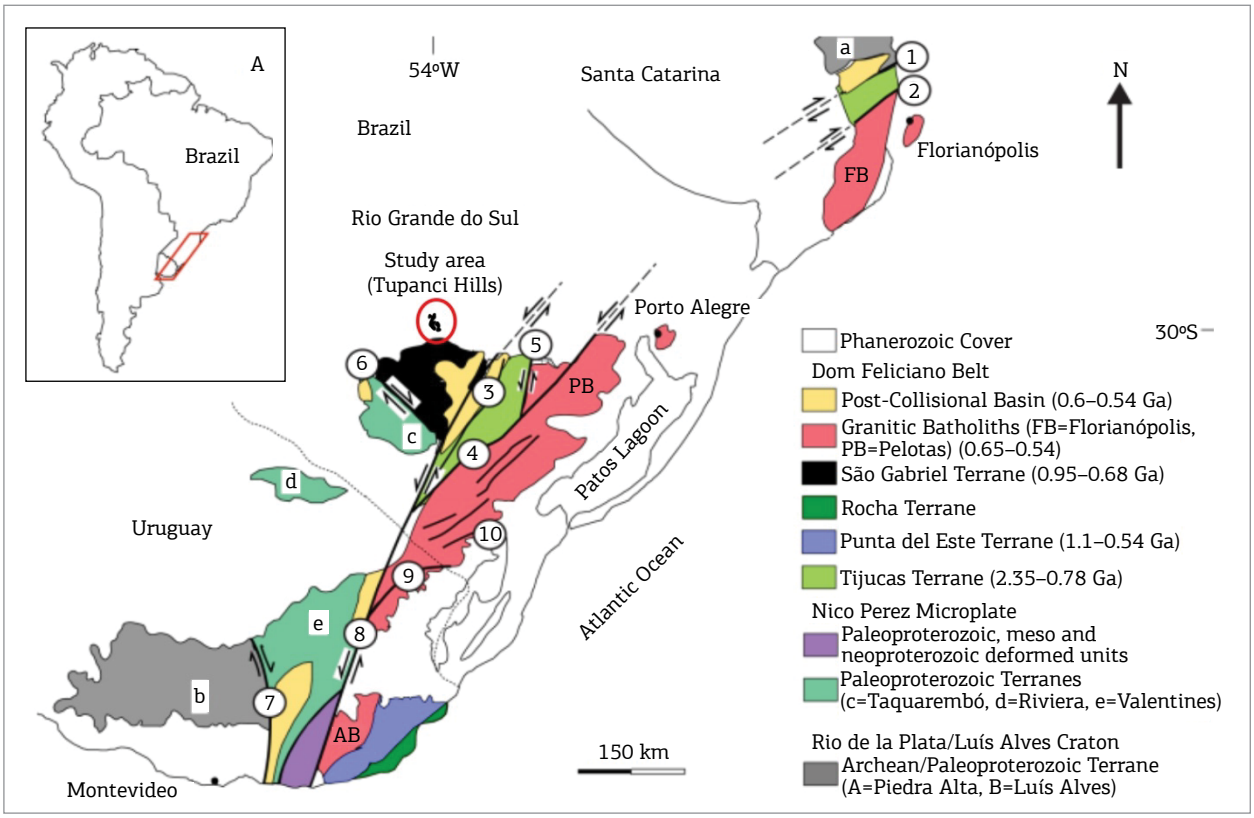

Figure 1. Simplified geological map of the Sul-Rio-Grandense Shield and Uruguay Shield (*cf.* Oyhantçabal *et al.* 2011), with location of the northernmost exposure of the Acampamento Velho volcanism in the Tupanci region (modified from Philipp *e t al.* 2016: Ductile Shear Zones: 1) Itajai-Perimbó, 2) Major Gercino, 3) Caçapava do Sul, 4) Dorsal de Canguçu, 5) Passo do Marinheiro, 6) Ibaré, 7) Sarandí del Yí, 8) Sierra Ballena, 9) Cerro Amaro, 10) Arroio Grande).

under subaerial conditions and has been described in detail by Wildner *et al.* (2002) and Lima *et al.* (2007). The first volcanic episode was between 585–590 Ma (Janikian *et al.* 2008) and is dominantly characterized by intermediate rocks with shoshonitic affinity (Bom Jardim Group, Hilario Formation). This volcanic episode is followed by a bimodal volcanism with sodic mildly alkaline volcanism (Bom Jardim Group, Acampamento Velho Formation) and ages between 560–550 Ma at the Ramada Plateau (Matté *et al.* 2016, Sommer *et al.* 2005a) and 574 Ma at the Passo do Salsinho Region (Chemale Jr. 2000, Janikian *et al.* 2008). The Acampamento Velho Formation (AVF) is the extrusive counterpart of the voluminous granitic magmatism, mostly metaluminous with minor peralkaline components, generated in the Brasiliano–Pan African cycle (Nardi & Bonin 1991). This episode is mainly exposed in volcanic plateaus and ridges composed mostly of acid effusive and pyroclastic rocks with minor intermediate and basic components (Sommer *et al.* 2005a, Wildner *et al.* 2002, Almeida *et al.* 2002). Eruptive periods were initiated with explosive episodes and closed by effusive events (Sommer *et al.* 2006). The best exposures of this volcanic sequence are in the Ramada Plateau (Vila Nova do Sul City), Taquarembó Plateau (Dom Pedrito City), Bugio and Perau Hills (Caçapava do Sul area, Santa Bárbara Hill), besides the Tupanci region, the northernmost exposure of this volcanism in the SRGS. Although some research has been developed in the deposits of the Tupanci region (Menegotto & Medeiros 1976, Roisenberg *et al.* 1986, Leitzke *et al.* 2015), integrated and detailed geochemistry, geochronology and isotopic data are scarce for this area.

Therefore, this paper focuses on dating and isotope systematics of acid volcanic rocks from the AVF in the Tupanci region, Brazil. We present new zircon U-Pb geochronological data for the high-silica volcanic successions, which coupled with Sm-Nd-Pb isotope systematics, and whole-rock geochemistry from literature data, enabled to better constrain the magmatic source and genesis of acid volcanic associations that occur in neoproterozoic post-collisional tectonic settings.

GEOLOGICAL SETTING

The SRGS (Fig. 1) is the southern portion of the Mantiqueira Province, located in the Rio Grande do Sul state, Brazil (Almeida *et al.* 1981). This shield includes rocks related to Brasilian–Pan African neoproterozoic orogenic cycle and a metamorphic basement of paleoproterozoic age, constituted by remaining fragments of the Rio de la Plata Craton (Teixeira *et al.* 2004). Well-preserved volcano-sedimentary sequences linked to magmatism in the collisional and post-collisional stages of the Brasilian orogenic cycle (Sommer *et al.* 2005a) are grouped in the Camaquã Basin (CB).

The CB is a retroarc basin that includes a set of preserved sedimentary and volcanogenic units, which were deposited between 620 and 535 Ma (Brito Neves & Cordani 1991, Gresse *et al.* 1996, Brito Neves *et al.* 1999, Chemale Jr. 2000, Fragoso-César *et al.* 2000, 2003, Paim *et al.* 2000, Sommer *et al.* 2006, Janikian *et al.* 2008, 2012). The basement of the CB is heterogeneous and ranges from paleoproterozoic granulitic complex to associations of metamorphic and deformed igneous rocks related to the Brasiliano–Pan-African orogeny (Paim *et al.* 2000, Lima *et al.* 2007). The evolution of the CB includes an alternation between accumulation periods, with the predominance of volcano-sedimentary sequences and erosional periods. The sedimentary sequence of CB is represented (Borba *et al.* 2007) from base to top by:

- Maricá Formation, with marine and coast deposits;
- Bom Jardim Group, with alluvial deposits intercalated with andesites, acid effusive and pyroclastic rocks (Hilário and Acampamento Velho formations);
- Camaquã Group characterized by fluvial, lacustrine and aeolian continental deposits (Santa Barbara and Guaritas formations).

These stratigraphic units evolved mainly in continental environments and the volcanism under subaerial conditions (Wildner *et al.* 2002).

Volcanic cycles in the CB occurred during a transition between a collisional and post-collisional period developed from the Neoproterozoic III to the Early Cambrian during the Brasiliano–Pan-African orogeny. The magmatic source of these rocks is probably related to partial melting of a lithospheric mantle previously chemically affected by a subduction process (Nardi & Bonin 1991, Wildner *et al.* 1999, 2002, Nardi & Lima 2000, Almeida *et al.* 2005, Sommer *et al.* 2006). Sommer *et al.* (2005a, 2005b, 2006) suggest that these volcanic cycles represent preserved portions of a typical evolutionary sequence from a post-collisional magmatism (from Liégeois 1998), with shoshonitic affinity rocks in the early stages, chemically affected by subduction-related processes, followed by silica-saturated bimodal volcanic sequences, with sodic-alkaline affinity and finally by tholeitic rocks.

STUDY AREA

Samples analyzed in this study were collected at the Tupanci region, along the Tupanci and Picados hills, northwest

of the SRGS (Fig. 2). Acid igneous rocks occur as shallow intrusions (hypabyssal rocks) at the Tupanci Hill and as lava flows (porphyritic rhyolites) and pyroclastic deposits (ignimbrites) at the Picados Hill. In this section, we will summarize the main petrographic and geochemical features of both occurrences, which were studied in detail by Leitzke *et al.* (2015) and are necessary for the interpretation of new isotopic data reported in this study.

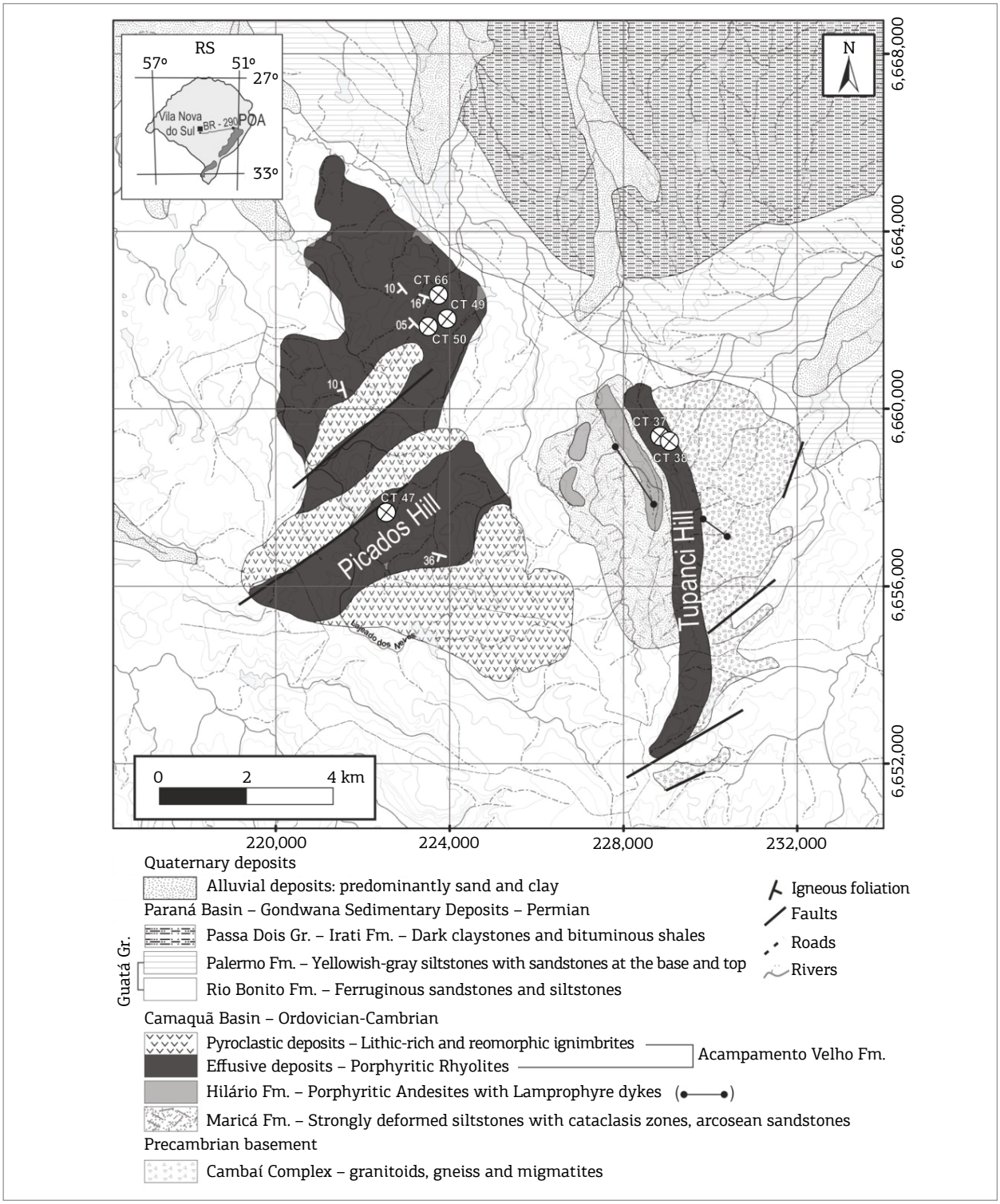

Figure 2. Simplified geological map of the study area with the location of the samples selected for this study (modified from Menegotto & Medeiros 1976 and Leitzke *et al.* 2015).

Summary of facies analysis, petrography and whole-rock geochemistry

Picados Hill area

Volcanic rocks in the Picados Hill area (Fig. 2) have effusive and explosive origin. The rhyolitic rocks are porphyritic, and the best outcrops are dominantly in the north-central portion of the hill. Pyroclastic rocks have a high degree of welding and predominate in the southern portion of the area. In this region lapilli-size fragments, with abundant lithic fragments, predominate. Predominantly, reomorphic portions are less abundant, being mostly ash-size crystal-rich fragments.

The effusive regime is characterized by porphyritic rhyolites with phenocrysts of quartz and sanidine set in an aphanitic glassy matrix (Figs. 3A-3D). Igneous flow foliation is mainly sub-horizontal and shows some autobrecciated portions (Fig. 3E). Microphenocrysts of opaque minerals, zircon and apatite occur as accessory minerals. Mafic minerals are predominantly biotite and chlorite, possibly originated by alteration of amphiboles. The biotite grains are subhedral, with diameter from 0.5–1 mm, ranging from brown to green and poikilitic texture. Biotite aggregates associated with chlorite has almost entirely replace amphibole crystals. The very fine matrix consists of a micro to cryptocrystalline quartz-feldsphatic arrange. Devitrification processes are common and several stages are observed, with spherulitic, axiolithic texture and granophyric intergrowths (Fig. 3F).

Explosive volcanism in the area is characterized by poorly selected ignimbrites with fragments ranging from ash to lapilli size, consisting of rock, crystal and glass fragments (Fig. 4). The ignimbrites are strongly welded and have rhyolitic composition. These rocks may be divided into two facies: lithic-rich ignimbrites (IgL); and rheomorphic crystal — rich ignimbrites (IgnReo).

The IgL corresponds to poorly selected brownish to pink color rocks with predominance of lapilli size fragments (Fig. 4A) immersed in a tuffaceous matrix. Lithic fragments are common and constituted by fragments of rhyolites and ignimbrites. Fragments of pumice (Fig. 4) occur in various sizes in the matrix and as lapilli fragments (Fig. 4). They are devitrified to a quartz-feldpathic granophyric arrangement with a low degree of flatenning, even though in some portions of the rock it is possible to identify an incipient eutaxithic texture. Alteration processes leave a reddish-brown clay-rich layer over the fragments. Quartz and alkali-feldspar crystal fragments are few. These mineral phases also occur as phenocrysts, with similar sizes, subhedral to euhedral and some of them preserved within the pumices. The matrix is extremely fine and supported by shards with spike geometry, with lengths smaller than 0.5 mm (Fig. 4B).

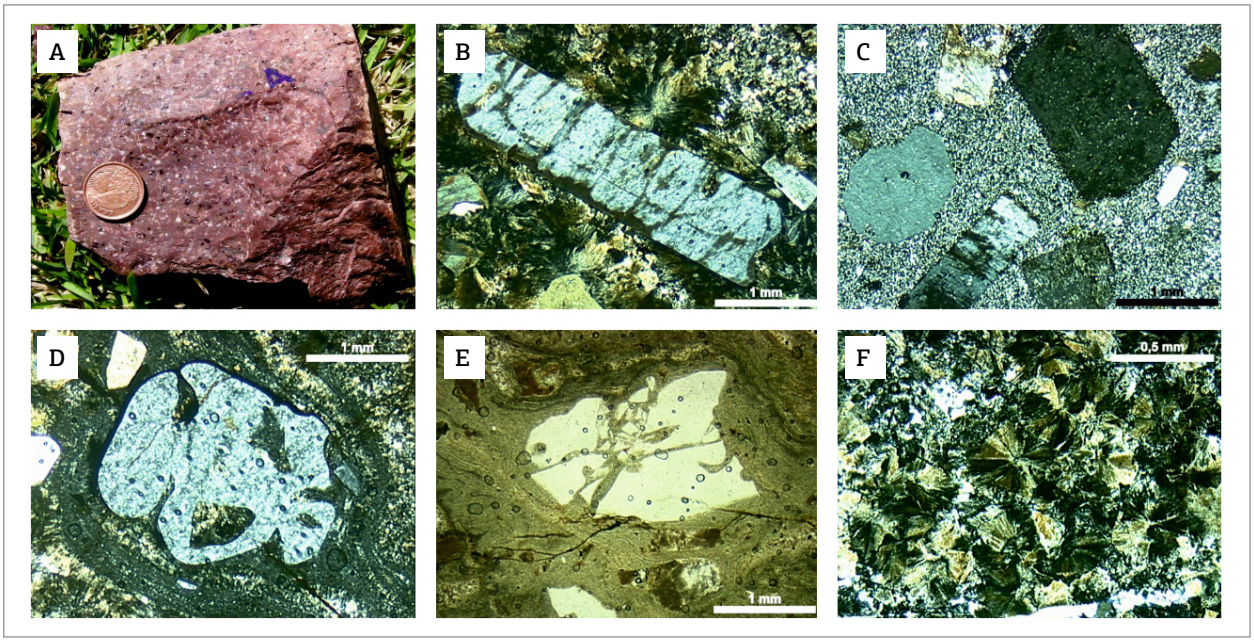

Figure 3. Summary of macro and microscopic features of representative effusive rocks at the Tupanci and Picados Hill (*cf.* Leitzke *et al.* 2015): (A) porphyritic rhyolite with glassy matrix; (B) fractured sanidine phenocryst in devitrified matrix; (C) glomeroporphyritic texture with euhedral quartz and k-feldspar phenocrysts; (D) reabsorbed quartz phenocryst with surrounding igneous flow foliation; (E) quartz phenocryst with microbreccia features; (F) spherulites showing evidence for high-temperature devitrification of the matrix.

Rheomorphic ignimbrites in the area are characterized by high degrees of welding (Fig. 4C) and a great amount of crystal fragments (phenocrysts and fragments) in a very fine-grained eutaxithic and often parataxithic matrix. These factors can be used to characterize them as "lava-like" ignimbrites (Ekren *et al.* 1984). Pyroclastic fragments are predominantly represented by quartz and alkali feldspar and stretched/deformed pumices (Fig. 4D). The lithic fragments are rare and, when observed, have rhyolitic composition. Pumice fragments are flattened (fiamme) and devitrified to quartz-feldspar aggregates.

Tupanci Hill area

The Tupanci Hill area comprises a N-S elongated subvolcanic body with a dominant NE-SW fault pattern. The main lithology is represented by porphyritic rhyolites with phenocrysts of sanidine and quartz surrounded by an equigranular-fine-grained to aphanitic quartz-feldspar matrix, with a strong flow foliation on border regions, where phenocrysts are substantially smaller in size. Spherulites occur in the matrix or around phenocrysts, showing evidence for high-temperature devitrification processes (Logfren 1971). Microphenocrysts of opaque minerals (pyrite), zircon, apatite and altered mafic minerals occur as accessories. Mafic minerals are rare and occur altered to chlorite. Small (≈ 0.05 mm) acicular crystals of late crystallization sodic amphibole (arfvedsonite) occur in the matrix, suggesting a peralkaline affinity. Fragments of sedimentary wall rocks of the Maricá Formation occur as xenoliths. Microfolded portions, rotated and fractured crystals (*microbreccias*) are also observed on the border of the intrusion, generating "tuff-like" textures similar to eutaxitic and parataxitic textures in pyroclastic rocks (Manley 1995), common in rhyolitic systems due to the high viscosity of the flow (Figs. 4E and 4G).

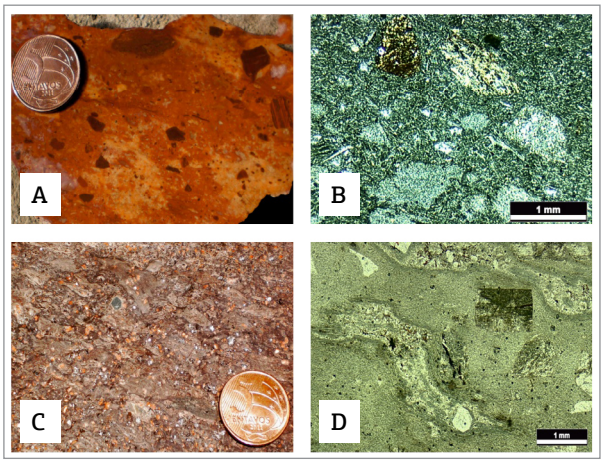

Figure 4 – Summary of macro and microscopic features of representative pyroclastic rocks at the Picados Hill (*cf.* Leitzke *et al.* 2015): (A) lapilli-size pyroclastic fragments in hand specimen; (B) pumice fragments with distinct orientations in a shard-based matrix; (C) highly-welded ignimbrite with eutaxitic texture of the pumice fragments; (D) stretched pumice fragments with eutaxitic texture and inclusions of quartz crystals under the microscope.

Whole-rock geochemistry

The geochemical features of both groups of rocks were described in detail by Leitzke *et al.* (2015) and are similar for major elements, but show distinct aspects regarding trace elements. The rocks have high contents of SiO_2 (73 to 77 wt.%), alkalis (Na_2O+K_2O > 8.4 wt.%) and FeO_t/(FeO_t+MgO) (> 0.9); with low contents of Al_2O_3, CaO and MgO; and agpaitic index close to the unity (> 0.9). At the Nb/Y *versus* Zr/TiO_2 classification diagram, these rocks are classified as rhyolites, which are confirmed by the Zr/TiO_2 *versus* SiO_2 diagram, in which some samples are classified as alkali rhyolites (Fig. 5). Major and trace elements data allowed the identification of two different evolutionary trends: low and high-Ti, related respectively to the effusive/pyroclastic rocks of the Picados Hill and subvolcanic rocks of Tupanci Hill (Leitzke *et al.* 2015). The same behavior is observed for trace and rare earth elements (REE) in multi-element variation diagrams. Zr contents are higher than 500 ppm for the high-Ti group that indicates, according to Leat *et al.* (1986), a peralkaline affinity for these rocks. On the other hand, the low-Ti group has Zr contents not higher than 420 ppm. Ba and Sr contents are > 70 and 8 ppm in the high-Ti group and < 16 and 6 ppm, respectively. Rb displays high contents in both groups, but concentrations are much higher in the low-Ti group (> 170 ppm) than in the high-Ti group (< 100 ppm). Nb, Y and Ga behave in a similar way, with higher contents for the low-Ti group (> 50, 130 and 25 ppm) compared to the high-Ti group (< 30, 70 and 26 ppm). High contents of Zr, Nb, Y, Ga and Rb and low contents of Ba and Sr for rocks of both groups (*cf.* Leitzke *et al.* 2015) are characteristic of acid magmatism with alkaline affinity (Pearce *et al.* 1984, Whalen *et al.* 1987, Nardi 1991).

ANALYTICAL PROCEDURES

This work presents a new isotopic dataset (zircon U-Pb, Sm-Nd and Pb-Pb) obtained on volcanic and hypabyssal rocks from the Tupanci area, which are coupled to whole-rock geochemistry data (Leitzke *et al.* 2015) to provide a better understanding of the evolution of the Acampamento Velho volcanism in the SRGS. Two samples of the Tupanci Hill (TH), which belong to the high-Ti group and consist

of porphyritic rhyolites, were selected for isotope analysis and one for zircon U-Pb dating (CT-38). In the Picados Hill (PH), three samples of the low-Ti group were selected for isotope determination. Additionally, a porphyritic rhyolite (sample CT-66) was selected for zircon U-Pb geochronology. Location of selected samples for the U-Pb zircon separation and isotopic measurement are given in Figure 2. Isotopic analyses were conducted at the University of São Paulo (USP) and at the Federal University of Rio Grande do Sul (UFRGS), and are described in detail in the following sections.

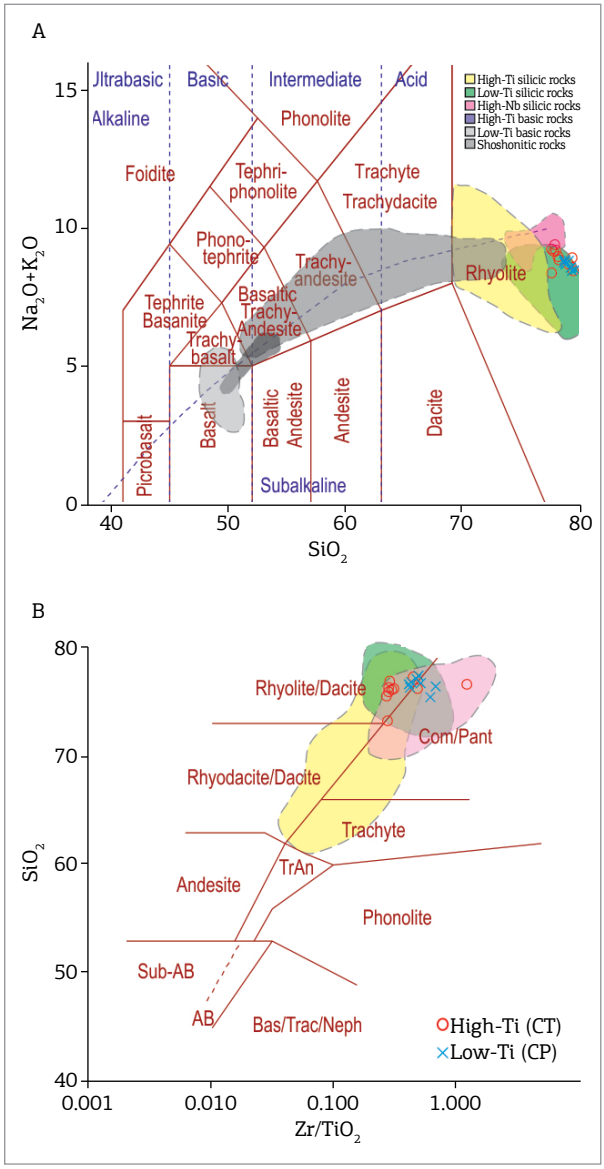

Figure 5. Classification diagrams for the high and low-Ti groups of silicic rocks from the Acampamento Velho Formation with comparisons between both groups at the Tupanci region and other occurrences of the post-collisional volcanism in southern Brazil. Data taken from Leitzke *et al.* (2015), and Sommer *et al.* (2005a): (A) TAS diagram (Le Bas *et al.* 1986); (B) SiO_2 *vs.* Zr/TiO_2 classification diagram (Winchester and Floyd 1977).

Zircon U-Pb geochronology (U-Pb LA-ICP-MS)

Approximately 0.5 kg of sample material was crushed, pulverized and sieved for zircon separation. The zircon grains were concentrated using conventional magnetic and heavy liquid techniques, after which more than 300 grains were handpicked and mounted in epoxy resin. From this population, 13 grains were analyzed from the high-Ti group (sample CT-38) and five grains from the low-Ti (sample CT-66).

The mount was polished using different granulometric pastes of diamond to expose the internal surfaces of the zircon. For the dating, the zircon grains were imaged using backscattered electrons and cathodoluminescence to determine their internal structures and crystallization phases. Only zircon grains without imperfections, fractures, and mineral inclusions were selected for isotopic analyses. All U-Pb isotopic analyses were performed at the Geochronological Research Center of the Geoscience Institute, USP, using a Thermo Fischer Scientific Neptune inductively coupled plasma-mass spectrometer (ICP-MS) and a 193 nm excimer laser ablation (LA) system (Photon Machines - Redmond, Washington, USA).

The details of the ICP-MS configurations and the laser parameters used during the analyses are available in Oliveira *et al.* (2015). The analytical procedure of the U-Pb method included the analysis of the materials in the following sequence: two blanks, two synthetic glass NIST standards , three external reference materials, 13 samples, two external reference materials, and two blanks. Each experiment consisted of 40 cycles of 1 s/cycle. The ^{204}Hg interference for ^{204}Pb was corrected using ^{202}Hg, in which $^{204}Hg/^{202}Hg = 4.2$. Both NIST glass and external reference material were used to normalize the $^{207}Pb/^{206}Pb$ ratio, whereas the external reference material was used to normalize the $^{238}U/^{206}Pb$ ratio. The standard GJ-1 (602 ± 4.4 Ma; Elhlou *et al.* 2006) was used as the external reference material. Zircon typically contains low concentrations of common Pb. Thus, the reliability of the measured $^{207}Pb/^{206}Pb$ and $^{238}U/^{206}Pb$ ratios critically depends on accurately assessing the common Pb component. The residual common Pb was corrected based on the measured ^{204}Pb concentration using the known terrestrial composition (Stacey & Kramers 1975).

External errors were calculated using error propagation for the individual measurements of the standard GJ-1 and the individual zircon sample measurements (spots). The ages were based mainly on $^{238}U/^{206}Pb$ and $^{207}Pb/^{206}Pb$ ratios and calculated through Isoplot software version 4.0 (Ludwig 2008).

More details of the analytical methods and data handling are available in Chemale Jr. *et al.* (2011).

Sm-Nd and Pb isotopic measurements

Isotopic analyses of Sm, Nd and Pb were carried out at the Isotope Geology laboratory of the UFRGS by thermal ionization mass spectrometry using a VG Sector 54 multicollector mass spectrometer. Whole rock samples were powered in agate mortar in order to get fraction lower than 200 mesh. Then, the samples were digested together with a $^{149}Sm/^{150}Nd$ spike through concentrated HF-HNO_3 and HCl in 7 mL teflon vials in a hot plate for seven days. After complete digestion, the samples were dried down and redissolved in 2.5 N HCl, and the REE were separated by using standard cation exchange chromatography with a DOWEX AG 50X8 resin (200–400 mesh) using 6 N HCl. Nd and Sm were separated from the other REE by using HDEHP LN resin (50–100 mm) and collected after elution with 0.18 N HCl for Nd and 0.5 N HCl for Sm. Pb was separated using DOWEX AG 1X8 resin (200–400 mesh) with 0.6N HBr and 6 N HCl. The isotopic analyses were carried out in static mode. Sm and Pb were run on Re single filaments, while Nd isotopes were loaded on Ta-Re-Ta triple filaments. Sm, Nd and Pb were deposited with H_3PO_4, and the latter was also deposited with silica gel. Nd isotopic ratios were normalized to $^{146}Nd/^{144}Nd = 0.7219$ and repeated measurements of La Jolla Nd reference material furnished a mean $^{143}Nd/^{144}Nd$ value of 0.511848 ± 0.000021 (1s; n = 100). Pb was corrected from a mass discrimination effect of 0.1% amu^{-1} based on 38 analyses of NBS-981 reference material. The total procedure blanks were lower than 500 pg for Sm, 150 pg for Nd, and 100 pg for Pb. Typical analytical errors for $^{147}Sm/^{144}Nd$ and $^{206,207,208}Pb/^{204}Pb$ ratio were equal or better than 0.1%. Nd-T_{DM} model ages were calculated according to De Paolo (1981). The decay constants recommended by Steiger and Jäger (1977) and Wasserburg *et al.* (1981) were used. The error for all isotopic data were lower than 25 ppm for Sm/Nd; 20 ppm for $^{143}Nd/^{144}Nd$; and lower than 0.0020 (SD absolute) for Pb isotopic analyses.

RESULTS

Zircon morphology and U-Pb results

The zircon populations comprise elongate, prismatic, subrounded grains, rarely showing well-preserved bipyramidal faces. These grains show low length-to-width ratios from 2:1 to 14:1 (with the average of 5:1), which are characteristics for deep-seated and slowly cooled intrusions (Corfu *et al.* 2003). Such morphological features suggest that zircon grains selected for the analysis are magmatic. Cathodoluminescence (CL) images of selected zircon grains (Fig. 6) from each sample allowed the recognition of inclusions and fractures and metamictic domains, which were avoided during the analyses, whenever possible. Some zircon grains display darker cores developed during magmatic crystallization. Zircon crystals from sample CT-66 show clear signs of alteration (Fig. 6) and high contents of common lead (14 to 59%), which affected negatively on the ages obtained for this group of analysis.

High-Ti rhyolite (sample CT-38)

Zircons from this sample are bright when analyzed through CL, although a few zircons exhibit either dark rims or dark cores (Fig. 6A). The U-Pb analytical data are presented in Table 1 and plotted in Concordia diagram (Tera & Wasserburg 1972), based on $^{207}Pb/^{206}Pb$ *versus* $^{238}U/^{206}Pb$ (Fig. 7A). All the zircon crystals have very high contents of U (1,679–4,296 ppm) and Th (1,089–4,086 ppm), but common Pb is still very low. Thirteen analyzed zircon yield a range in the $^{206}Pb/^{238}U$ ages from 559 to 605 Ma and all the analytical points are concordant. Therefore a Concordia age of 579 ± 5.6 Ma (mean square weighted deviation - MSWD = 0.16) has been calculated using these zircons (Fig. 7A), which is interpreted as the crystallization age of this sample.

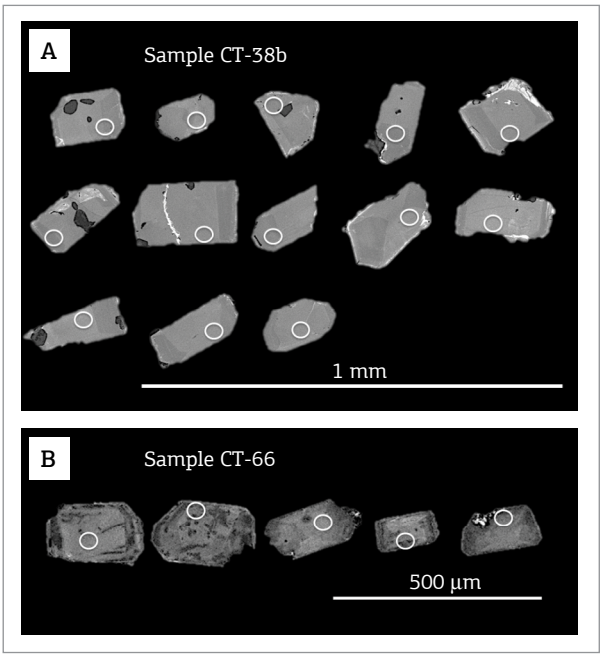

Figure 6. Cathodoluminescence images of zircons from the (A) Tupanci Hill, with internal zonation due to crystal growth during magma cooling, and (B) Picados Hill, which show features of alteration. White circles show where LA-ICP-MS analysis were performed.

Low-Ti rhyolite (sample CT-66)

Zircon grains from this sample are invariably dark with many inclusions and no discernible zoning. When compared to the sample CT-38, these zircons are not as clear, which reflect hydrothermal alteration (Fig. 6B). A few zircons exhibit locally either dark rims or dark cores (Fig. 6B). The U-Pb analytical data are presented in Table 1, and plotted in the conventional Concordia diagram (Whetherill 1956) based on $^{238}U/^{206}Pb$ *versus* $^{207}Pb/^{235}U$ (Fig. 7B). The five analyzed fractions yield a range in the $^{207}Pb/^{206}Pb$ ages from 553 to 588 Ma and are discordant. A Discordia (Fig. 7B) using the five fractions yields an upper intercept at 558 ± 39 Ma with a low MSWD (0.70). This high error is due to the small number of crystals used for dating associated with the high content of uranium, which may have been lost due to alteration and deterioration of the crystalline reticulum.

Sm-Nd isotopic results

For Sm-Nd whole-rock determination and T_{DM} age calculation, five samples were selected:

- Two from the high-Ti rhyolites of the Tupanci Hill (CT-37A, CT-37B);
- Three samples from the low-Ti rhyolites of the Picados Hill (CT-47A, CT-49A, CT-50A).

Table 2 shows the Sm-Nd isotopic results as well as the initial e_{Nd} values calculated at the time of emplacement, which is yielded by the zircon U-Pb ages obtained in this study. For the high-Ti samples, a crystallization age of 579 Ma is assumed, while the age of 558 Ma is assumed for the emplacement of the low-Ti rhyolites.

The set of results provided T_{DM} model ages of 1.83 and 2.22 Ga and more negative present day $e_{Nd(0)}$ values of -17.47 and -18.00 for the high-Ti rhyolites, while the low-Ti rhyolites exhibit negative $e_{Nd(0)}$ values from -10.43 to -9.60. The $e_{Nd(t)}$ of the high-Ti samples are of -12.15 and -11.15, while low-Ti samples show $e_{Nd(t)}$ ranging from -11.21 to -10.09. The high-Ti rhyolites displayed homogeneous $^{147}Sm/^{144}Nd$ ratios of 0.125 and 0.104, which are within the 0.080–0.120 range, usually considerable acceptable for T_{DM} age calculation. On the other side, the samples of the low-Ti rhyolites have unusually

Table 1. U-Pb LA-ICP-MS data for zircon grains from the silicic volcanic and hypabyssal rocks in the northernmost exposures (low and high-Ti) of the Acampamento Velho Formation in the NW portion of the Sul-Rio-Grandense Shield.

Sample (Group)	Grain spot	$^{206}Pb_c$ (%)	U (ppm)	Th (ppm)	^{206}Pb (ppm)	$^{232}Th/^{238}U$	$^{206}Pb/^{238}U$ (age-Ga)	1σ (%)	$^{207}Pb/^{206}Pb$ (age-Ga)	1σ (%)	$^{207}Pb/^{206}Pb$	1σ (%)	$^{207}Pb/^{235}U$	1σ (%)	$^{206}Pb/^{238}U$	1σ (%)	Err. Corr.
CT-38 (High-Ti)	1.1	0.21	3114	2168	385	0.696	0.585	1.20	0.570	9.47	0.0591	2.54	0.7741	2.62	0.0950	1.26	0.97
	2.1	0.11	2173	1505	278	0.693	0.586	1.19	0.582	10.65	0.0594	2.86	0.7801	2.92	0.0952	1.26	0.99
	3.1	0.22	2562	1627	304	0.635	0.579	1.21	0.559	10.38	0.0588	2.72	0.7612	2.82	0.0939	1.28	0.92
	4.1	0.09	3025	2615	401	0.864	0.559	1.25	0.562	9.79	0.0589	2.55	0.7351	2.76	0.0906	1.32	0.98
	5.1	0.22	2648	1601	335	0.605	0.573	1.32	0.568	9.86	0.0590	2.54	0.7569	2.72	0.0930	1.29	0.98
	6.1	0.04	2973	2296	397	0.772	0.575	1.25	0.574	9.76	0.0592	2.53	0.7606	2.70	0.0932	1.29	0.97
	7.1	0.18	2307	1463	277	0.634	0.561	1.16	0.581	10.15	0.0594	2.69	0.7439	2.93	0.0909	1.32	0.97
	8.1	0.10	2348	1440	301	0.613	0.605	1.20	0.585	9.57	0.0595	2.52	0.8075	2.65	0.0984	1.22	0.95
	9.1	0.58	1679	1089	209	0.648	0.581	1.22	0.561	11.05	0.0588	2.89	0.7644	2.90	0.0942	1.27	0.96
	10.1	0.33	2377	1633	285	0.687	0.576	1.25	0.576	9.20	0.0593	2.53	0.7630	2.63	0.0934	1.28	0.91
	11.1	0.03	4296	4086	549	0.951	0.560	1.19	0.570	8.95	0.0591	2.37	0.7389	2.61	0.0907	1.21	0.98
	12.1	0.09	2634	1483	334	0.563	0.590	1.18	0.569	9.67	0.0591	2.54	0.7806	2.65	0.0959	1.25	0.95
	13.1	0.03	2219	1536	298	0.692	0.594	1.16	0.583	9.95	0.0594	2.69	0.7914	2.77	0.0966	1.24	0.98
*CT-66 (Low-Ti)	1.1	14.39	2780	2237	333	0.800	0.692	1.15	0.588	5.78	0.0596	1.51	0.9311	1.94	0.1134	1.23	0.99
	2.1	23.69	3510	2811	448	0.800	0.607	1.11	0.580	5.52	0.0594	1.52	0.8082	1.78	0.0987	1.22	0.88
	3.1	30.65	3844	4018	588	1.050	0.632	1.03	0.572	5.42	0.0591	1.35	0.8394	1.82	0.1029	1.17	0.92
	5.1	58.71	2180	1773	317	0.810	0.677	1.05	0.558	6.09	0.0588	1.53	0.8967	1.77	0.1107	1.08	0.92
	4.1	18.20	2396	1704	268	0.710	0.572	1.13	0.553	6.51	0.0586	1.71	0.7496	1.87	0.0927	1.19	0.97

*Sample with high content of common $^{206}Pb_c$. 1σ expressed in %.

high $^{147}Sm/^{144}Nd$ ratios of 0.205–0.207, which is close to the value of depleted mantle ($^{147}Sm/^{144}Nd$ = 0.225) and normally found in mafic rocks, which led to difficulties in interpreting model ages. The uncertainty in the age increases dramatically as the $^{147}Sm/^{144}Nd$ ratio of the samples approaches that of the depleted mantle. In this study, therefore, following the work of Harris *et al.* (1994) and DePaolo (1981), model ages obtained from samples with high $^{147}Sm/^{144}Nd$ ratios (> 0.15) were not considered because they are unrealistic.

Pb isotope systematics results

The high-Ti rhyolites show present-day Pb isotope compositions of 15.971–16.141 for $^{206}Pb/^{204}Pb$; 15.113–15.128 for $^{207}Pb/^{204}Pb$, and 37.009–37.089 for $^{208}Pb/^{204}Pb$. The low-Ti rhyolites display slightly lower Pb isotope ratios compared to the high-Ti rocks, although the $^{206}Pb/^{204}Pb$ ratios are within the same range. The ratios are 15.830–16.006 for $^{206}Pb/^{204}Pb$; 15.062–15.097 for $^{207}Pb/^{204}Pb$; and 36.567–36.862 for $^{208}Pb/^{204}Pb$ (Table 2).

DISCUSSION

Timing and emplacement of volcanic episodes of the Acampamento Velho Formation in the NW of the SRGS

Recent geochronological literature data provided ages between 549 and 573 Ma (Tab. 3) for the volcanic rocks of the AVF. At the Passo do Salsinho region, U-Pb SHRIMP zircon analysis in rhyolitic lavas revealed ages of 573 ± 18 Ma (Chemale Jr. 2000). Similar and more precise results of 572 ± 3 Ma were obtained through Pb/Pb isotopic ratio in zircon grains from granitoids of the Leões Ring Complex (Gastal & Lafon 2001). These granitoids are genetically associated with the volcanic rocks of the Taquarembó Plateau. U-Pb zircon analysis in volcanic rocks of the Ramada Plateau provided the age between 549 and 560 Ma to the AVF volcanism, which suggests a greater time span for this volcanic episode in the SRGS (Sommer *et al.*

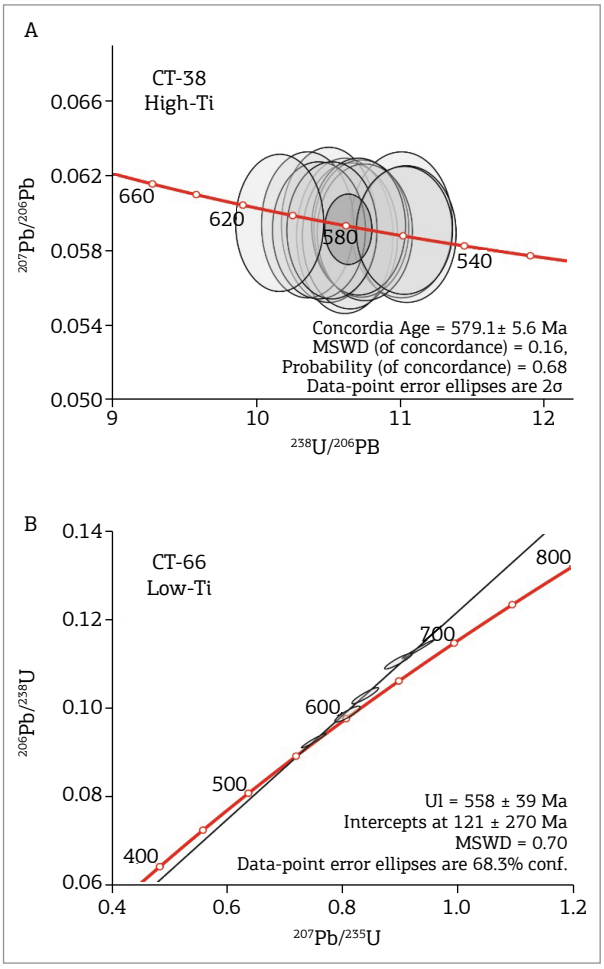

Figure 7. U–Pb Concordia diagrams displaying obtained data from zircons of the AVF high (A) and low (B) -Ti rhyolites at the Tupanci region, NW of the Sul-Rio-Grandense Shield.

Table 2. Isotopic results for the silicic volcanic and hypabyssal rocks in the northernmost exposure of the Acampamento Velho Formation in the NW portion of the Sul-Rio-Grandense Shield.

Group	Sample	$^{206}Pb/^{204}Pb$	2σ	$^{207}Pb/^{204}Pb$	2σ	$^{208}Pb/^{204}Pb$	2σ	Sm (ppm)	Nd (ppm)	$^{147}Sm/^{144}Nd$	$^{143}Nd/^{144}Nd$	Error	εNd (0)	εNd (t)	T_{DM} (Ga)
High-Ti	CT-37A	16.140	0.002	15.128	0.001	37.089	0.002	10.19	49.41	0.1247	0.511743	0.000015	-17.47	-12.15	2.22
	CT-37B	15.971	0.002	15.113	0.001	37.009	0.001	14.73	85.71	0.1039	0.511715	0.000007	-18.00	-11.15	1.83
Low-Ti	CT-47A	15.923	0.001	15.062	0.001	36.590	0.001	7.22	21.20	0.2058	0.512146	0.000009	-9.6	-10.09	-
	CT-49A	16.007	0.001	15.097	0.001	36.862	0.001	11.81	34.49	0.2070	0.512103	0.000015	-10.43	-11.21	-
	CT-50A	15.823	0.002	15.066	0.001	36.567	0.002	11.37	33.50	0.2052	0.512131	0.000011	-9.88	-10.53	-

εNd (t) was calculated on basis in the crystallization age of 579 Ma.

2005b, Matté *et al.* 2016). Analysis of two rhyolitic pebbles from the conglomeratic fluvial deposits of the basal portion of the AVF provided zircon U-Pb ages of 579 ± 13 Ma and 569 ± 2.4 Ma (Janikian *et al.* 2012). However, these authors proposed the individualization of a new younger acid volcanic unit related to reactivation of extensional structures identified in Taquarembó Plateau, for which the crystallization age, obtained by U-Pb LA-ICP-MS method in lapilli-tuffs previously considered as part of the AVF, is 544.2 ± 5.5 Ma (Wildner *et al.* 1999, 2002, Sommer *et al.* 2006). This was correlated with the U-Pb zircon SHRIMP age of 549.3 ± 5 Ma obtained by Sommer *et al.* (2005a) in hypabyssal rhyolites of the Ramada Plateau. The new age of 579 ± 5 Ma of the high-Ti rhyolites from the AVF obtained in this study is in agreement with those ones previously obtained in the literature (Chemale Jr. 2000, Janikian *et al.* 2005, 2008, Gastal & Lafon 2001, Sommer *et al.* 2005a, 2006). For the age of 558 ± 39 Ma obtained in the low-Ti group, the high uncertainty associated with the data may indicate an overlap with the ca. 570 Ma event of the AVF, or suggest a younger volcanic episode at the Camaquã Basin (*cf.*, Janikian *et al.* 2012, Matté *et al.* 2016).

Trace element geochemistry indicates that rocks from the high-Ti group were likely generated in a post-collisional setting, while those ones of the low-Ti group were generated in a progressive post-collision to intraplate setting (*cf.* Leitzke *et al.* 2015). Assuming this, it is expected that our geochronological results are coherent with the tectonic environment, and, therefore, show distinct ages between both groups. Nevertheless, the poorly constrained age for the low-Ti group still does not allow to confirm the tectonic environment distinction between both groups. Regarding whole-rock trace element patterns, both high and low-Ti groups have high contents of HFSE (Zr, Nb, Y), Ga and Rb, together with lower contents of Ba and Sr (Fig. 8A), characteristic of acid magmatism with an alkaline affinity, typical of final stages of orogenic cycles, with sources previously affected by subduction-related metasomatism (Pearce *et al.* 1984, Whalen *et al.* 1987, Nardi 1991, Sommer *et al.* 2005a). The magmatism of the AVF has been recognized to be produced from subduction-modified mantle sources, likely of EM1 type, during the final stages of Brasiliano–Pan-African cycle (Wildner *et al.* 2002). Moreover, the origin of the rhyolitic liquids has been modelled to be fractional crystallization of plagioclase+alkali feldspar+pyroxene+-magnetite from trachytic magmas, which, in turn, are produced by differentiation of mildly alkaline basaltic magmas (Sommer *et al.* 1999, Matté *et al.* 2012). Shellnutt *et al.* (2009) use the Th/Ta ratio to indicate to which extent the interaction crust-mantle was present during the petrogenesis of an igneous association of rocks. This ratio should be around 2.0 produced exclusively by mantle partial melting, while it should be greater than 6.9 to the ones originated by crustal partial melting. In our high-Ti group (CT) Th/Ta > 6.9 predominates, while at our low-Ti group (CP) the values range between 6.9 and 4.2, indicating crustal contribution to their origin. According to Eby (1990, 1992), the fractionation of "A" type magmas has little effect on the Y/Nb ratio, which could also be used to indicate the source

Table 3. Summary of geochronological data available in the literature for the Acampamento Velho volcanism and comparison with results from this study.

Outcrop	Type of rock	Age (Ma)	Error (Ma)	Method	Reference
Ramada Plateau	Subvolcanic rhyolite	549.0	5.0	U-Pb SHRIMP	Sommer *et al.* (2005)
Ramada Plateau	Diorite	550.2	1.5	U-Pb LA-ICP-MS	Matté *et al.* (2011)
Taquarembo Plateau	Acid tuff	553.0	17.0	U-Pb LA-ICP-MS	Janikian *et al.* (2012)
Bugio Hill	Basalt	553.0	5.0	U-Pb LA-ICP-MS	Almeida *et al.* (2012)
Eastern Ramada Plateau	Rhyolitic Ignimbrite	560.0	2.0	U-Pb LA-ICP-MS	Matté *et al.* (2016)
Eastern Ramada Plateau	Subvolcanic trachyte	560.0	14.0	U-Pb LA-ICP-MS	Matté *et al.* (2016)
Ramada Plateau	Rhyolitic Ignimbrite	560.7	2.1	U-Pb LA-ICP-MS	Matté *et al.* (2016)
Eastern Ramada Plateau	Subvolcanic rhyolite	561.7	1.8	U-Pb LA-ICP-MS	Matté *et al.* (2016)
Taquarembo Plateau	Rhyolite	570.7	4.1	U-Pb LA-ICP-MS	Sommer *et al.* (in prep.)
Bom Jardim	Subvolcanic rhyolite	572.2	6.5	U-Pb LA-ICP-MS	Janikian *et al.* (2012)
Perau Hill	Rhyolite	573.0	18.0	U-Pb SHRIMP	Chemale Jr. (2000)
Ramada Plateau	Rhyolite	574.0	7.0	U-Pb TIMS	Janikian *et al.* (2008)
Tupanci Hill	**Rhyolite**	**579.1**	**5.6**	**U-Pb LA-ICP-MS**	**This study**
Picados Hill	**Rhyolite**	**558.0**	**39.0**	**U-Pb LA-ICP-MS**	**This study**

LA-ICP-MS: laser ablation inductively coupled plasma mass spectrometry; SHRIMP: sensitive high-resolution ion microprobe; TIMS: thermal ionization mass spectrometry.

of the magmatism. Mantle-derived magmas would have Y/Nb < 1.2, while those of crustal origin should have it > 1.2. These geochemical criteria would indicate crustal origin for both groups of acid volcanic rocks in this study, in which Y/Nb ranges from 1.6 to 4.1 (*cf.* Leitzke *et al.* 2015).

In both groups, REE are present in moderate to high concentrations (ΣREE = 198–694 ppm). The fractionation between light rare-earth elements (LREE) and heavy rare earth elements (HREE) is low for the low-Ti (CP) group (La_N/Yb_N = 1.7–6.9) and higher for the high-Ti (CT) group (La_N/Yb_N = 3.48–17.64). In general terms, the fractionation of LREE is more pronounced than HREE, with LaN/SmN (1.6–5.1) higher than TbN/LuN (1.2–1.5). In all samples, there is a strong negative Eu anomaly (Eu/Eu* = 0.01–0.19), related to its bivalent character and consequently previous fractionation into feldspars. As already observed for the AVF at the Ramada Plateau, the high-Ti rhyolites are enriched in REE, mainly LREE, when compared to the low-Ti group (Fig. 8B). These characteristics were also identified in other occurrences of the AVF at the SRGS (Sommer *et al.* 2005b, 2006), where low and high-Ti groups of basalts and rhyolites were identified. The magmatic source of these groups and their petrogenetic correlation are still not well constrained.

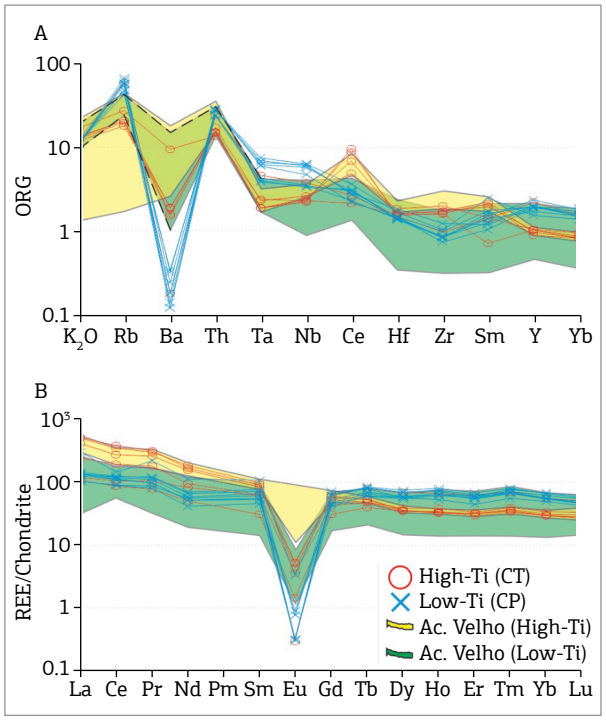

Figure 8. Multi-element diagram for the low and high-Ti groups of the Acampamento Velho Formation at the Tupanci region, NW of the Sul-Rio-Grandense Shield (*cf.* Leitzke *et al.* 2015) plotted together with literature data: (A) ORG-normalized (Pearce *et al.* 1984) trace element (+K_2O) pattern; (B) chondrite-normalized rare earth elements (REE) pattern (Nakamura 1974).

When compared to tectonic environment (Fig. 9) trace element patterns (*cf.* Pearce *et al.* 1984), the samples are divided accordingly to their group, with high-Ti rhyolites showing a post-collisional settings pattern, while the low-Ti are more likely related to intraplate granites, which is coherent with the increase of peralkalinity. In the granitoids classification diagram (Whalen *et al.* 1987), all the samples are classified as "A" type granites, which are by definition alkaline and anorogenic. This classification is confirmed by the (10^{4}*Ga)/Al > 2.6, Ce+Y+Nb+Zr > 500 ppm and FeOt/FeOt+MgO > 0.9, as proposed by Nardi and Bitencourt (2009) for the post-collisional granitic magmatism at the southern portion of Brazil. Nevertheless, when compared to other occurrences of the AVF, the rocks from the high-Ti group (CT) of the Tupanci area have lower contents of Rb, Nb, Y and higher of Zr and Ce when compared to the low-Ti group (CP), suggesting a different evolution for this group.

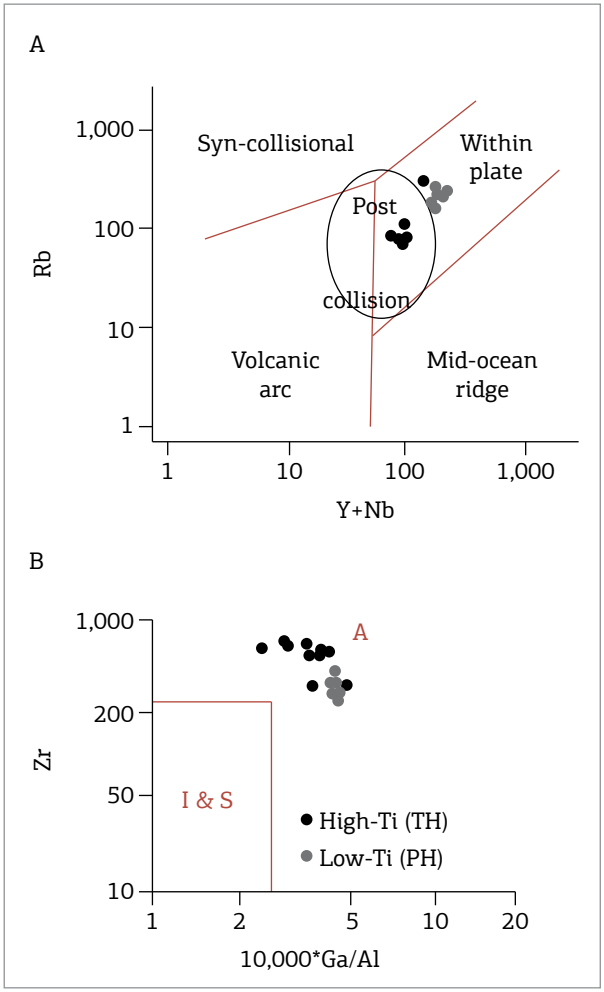

Figure 9. Tectonic discrimination diagram for the studied rocks (cf. Leitzke *et al.* 2015): (A) Rb *vs.* Y+Nb according to Pearce *et al.* (1984); (B) Zr *vs.* 10,000*Ga/Al (Whalen *et al.* 1987).

The new ages for the AVF at the Tupanci region, coupled with trace element content of the two volcanic sequences (Leitzke *et al.* 2015) are coherent with the tectonic environment expected for the different groups, suggesting that the high-Ti group was generated in a post-collisional setting, while the low-Ti group was generated in a progressive post-collision to intraplate setting. Our new ages for the high-Ti group at the Tupanci area agrees well with previous studies, while the age obtained to the low-Ti group, although with high uncertainty, may be related to different episodes of the Acampamento Velho volcanism in its northernmost exposure SRGS (*cf.* Janikian *et al.* 2012).

Constraints for the magmatic sources of the AVF volcanism based on Sm-Nd and Pb-Pb isotope systematics

The significance of negative ε_{Nd} and differences in the $^{147}Sm/^{144}Nd$ observed in acid lavas can be addressed to crust-derived lavas, or to crustal contamination of basaltic lavas during differentiation or metasomatic rocks (Almeida *et al.* 2005). According to the isotopic results, the high-Ti group would also represent a fraction of these volcanic episodes that had a greater component of crustal contamination, since it presents a slightly more negative εNd.

T_{DM} model ages (DePaolo 1981, 1988) ranging from 1.83 to 2.22 Ga for the high-Ti rocks are in agreement with the ones previously obtained (Chemale Jr. 2000, Almeida *et al.* 2005, Janikian *et al.* 2012), suggesting a contribution of paleoproterozoic basement in the source of these magmas (Fig. 10). Isotopic data obtained from rocks of the neoproterozoic plutono-volcanic alkaline association at the Taquarembó Plateau, that also belongs to the AVF (Wildner *et al.* 1999), suggest an EM1-type mantle source (Hart 1988). Chemale Jr. (2000) reported εNd (t = 570 Ma) values between -15 and -17 and $^{87}Sr/^{86}Sr_i$ ratios close to 0.7045, which are similar to the results obtained by Gastal and Lafon (1998) for intrusive rocks of alkaline associations in the SRGS, correlated to the Taquarembó Plateau magmatism. When coupled with major and trace elements geochemistry, our data suggest that the source of the Tupanci magmatism may also be a lithospheric mantle previously affected by subduction metasomatic processes. The ε_{Nd} *versus* time diagram (Fig. 10) compares the Nd isotopic evolution of the investigated rocks with distinct crusts (Rio Vacacaí Terrane, Santa Maria Chico Complex and Dom Feliciano Belt) from the SRGS (cf. Janikian *et al.* 2012). In this context, it is clearly seen that studied samples of the AVF show paleoproterozoic T_{DM} ages from Rhyacian to Statherian and plot in an intermediate position between the neoproterozoic (Rio Vacacaí Terrane) and the paleoproterozoic crusts (Dom Feliciano, Pinheiro Machado Suite and Encantada Gneisses).

The Pb isotope data (Fig. 11) of the studied samples suggest a significant crustal contribution with lower paleoproterozoic

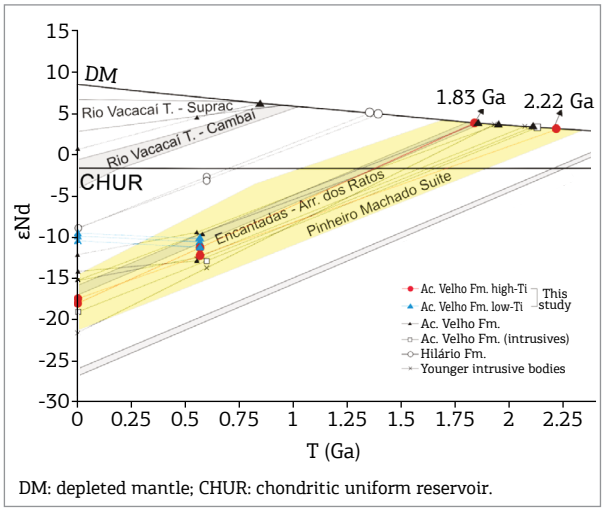

Figure 10. Diagram showing εNd *vs.* T (Ga) for the low and high-Ti rhyolitic rocks from the Acampamento Velho Formation at the Tupanci region, as well as their possible sources (modified from the compilation by Janikian *et al.* 2012).

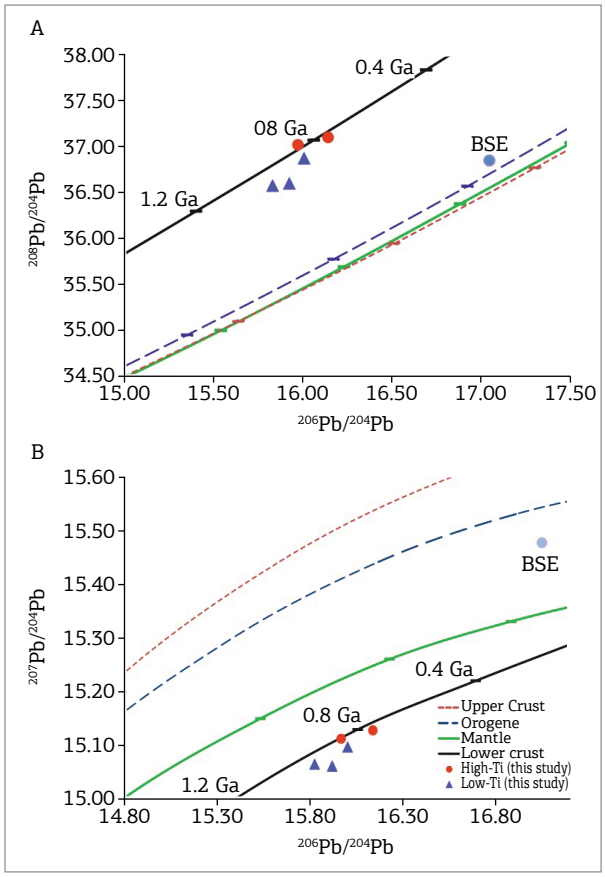

Figure 11. (A) $^{208}Pb/^{204}Pb$ *vs.* $^{206}Pb/^{204}Pb$; (B) $^{207}Pb/^{204}Pb$ *vs.* $^{206}Pb/^{204}Pb$ isotopic signatures for the low and high-Ti rhyolitic rocks from the AVF at the Tupanci region plotted together with possible end-member sources evolution with time (*cf.* Stacey & Kramers 1975).

crust melting related to the Dom Feliciano Complex. The high $^{147}Sm/^{144}Nd$ ratios of the low-Ti rocks coupled to the REE-chondrite normalized pattern observed is a feature produced in ultra-evolved silicic magmas attributed to magmatic fractionation, which may lead to an erroneous estimate of the Nd model age of the low-Ti rocks. Another possible explanation for the high $^{147}Sm/^{144}Nd$ in the low-Ti group could be related to a local source control, mineral sorting, with fractionation of minerals such as monazite, or hydrothermal alteration (Verma *et al.* 2005). Nevertheless, the similarity between εNd(t) for both rhyolite groups suggest a similar source, which may be a paleoproterozoic crust, as evidenced by the $^{143}Nd/^{144}Nd$ *vs*. time diagram.

CONCLUSIONS

New U-Pb ages obtained in zircon grains from high-Ti rhyolites from the AVF at the NW portion of the SRGS indicate an event at 579.1 +/- 5.6 Ma and are in good agreement with reported ages for the time span of the AVF volcanism in the Bom Jardim Group of the CB (*cf.* Chemale Jr. 2000, Janikian *et al.* 2005, 2008, Gastal & Lafon 2001). A second U-Pb age of 558 Ma was obtained for rhyolites from the low-Ti group at the Picados Hill, although with a high uncertainty associated (+/- 39 Ma) probably due to the high degree of alteration of the zircon grains. Nevertheless, more precise geochronological data reported recently in the literature may be used to indicate a younger acid volcanism, or a greater time span for the AVF volcanism in southernmost Brazil (Janikian *et al.* 2012, Matté *et al.* 2016), although the high uncertainty obtained in this study does not allow this issue to be conclusive. Regarding magmatic sources, Sm/Nd isotopic data coupled to Pb isotopes and trace element geochemistry of these rocks indicate variable amounts of paleoproterozoic lower crust melting, in a progressive post-collisional do intraplate environment. The high values for $^{147}Sm/^{144}Nd$ ratios of rocks from the low-Ti group are probably related to the fractionation of minerals or hydrothermal alteration of the samples. Our new data allows to better understand the stratigraphic evolution of the neoproterozoic post-collisional volcanic successions of the CB in the SRGS and the evolution of magmatic cycles during the late stages of the Brasiliano–Pan-African orogeny in southern Brazil.

ACKNOWLEDGMENTS

The authors acknowledge CNPq (303015/2015-2; 400724/2014-6, 441766/2014-5, 302213/2012-0, 303584/2009-2, 471402/2012-5, and 470505/2010-9), for research funding. We also acknowledge the referees for their constructive inputs. IGEO/UFRGS and CPGEO/USP are thanked for support during the field and laboratory work.

REFERENCES

Almeida D.P.M., Conceição R.V., Chemale Jr. F., Koester E., Borba A.W., Petry K. 2005. Evolution of heterogeneous mantle in the Acampamento Velho and Rodeio Velho volcanic events, Camaquã Basin, southern Brazil. *Gondwana Research*, **8**(4):479-492.

Almeida F.F.M., Hasui Y., Brito Neves B.B., Fuck R.A. 1981. Brazilian structural provinces: an introduction. *Earth-Sciences Review*, **17**(1-2):1-29.

Almeida D.P.M., Zerfass H., Basei M.A., Petry K., Gomes C.H. 2002. The Acampamento Velho Formation, a Lower Cambrian Bimodal Volcanic Package: Geochemical and Stratigraphic Studies from the Cerro do Bugio, Perau and Serra de Santa Bárbara (Caçapava do Sul, Rio Grande do Sul, RS – Brazil). *Gondwana Research*, **5**(3):721-733.

Babinski M., Chemale Jr. F., Van Schmus W.R., Hartmann L.A., Silva L.C. 1997. U-Pb and Sm-Nd geochronology of the neoproterozoic granitic-gneissic Dom Feliciano belt, Southern Brazil. *Journal of South American Earth Sciences*, **10**(3-4):263-274.

Bitencourt M.F. & Nardi L.V.S. 2000. Tectonic setting and sources of magmatism related to the Southern Brazilian Shear Belt. *Revista Brasileira de Geociências*, **30**(1):184-187.

Borba A.W., Maraschin A.J., Noronha F.L., Casagrande J., Mizusaki A.M.P. 2007. Provenance of the sedimentary rocks of the Bom Jardim Group (Neoproterozoic, southern Brazil): Evidence from petrography, geochemistry and Neodymium isotopes. *Latin American Journal of Sedimentology and Basin Analysis*, **14**:25-42.

Brito Neves B.B., Campos Neto M.C., Fuck R.A. 1999. From Rodinia to Western Gondwana: an approach to the Brasiliano–Pan African cycle and orogenic collage. *Episodes*, **22**(3):155-166.

Brito Neves B.B. & Cordani U.G. 1991. Tectonic evolution of South America during the Late Proterozoic. *Precambrian Research*, **53**(1-2):23-40.

Chemale Jr. F. 2000. Evolução Geológica do Escudo Sul-rio-grandense. *In:* De Ros L.F. & Holz M. (eds.) *Geologia do Rio Grande do Sul.* Porto Alegre, CIGO/UFRGS, p. 13-52.

Chemale Jr. F., Philipp R.P., Dussin I.A., Formoso M.L.L., Kawashita K., Berttotti A.L. 2011. Lu-Hf and U-Pb age determination of Capivarita Anorthosite in the Dom Feliciano Belt, Brazil. *Precambrian Research*, **186**(1-4):117-126.

Corfu F., Hanchar J.M., Hoskin P.W.O., Kinny P. 2003. Atlas of zircon textures. *In:* Hanchar J.M., Hoskin P.W.O. (eds.) *Reviews in Mineralogy & Geochemistry - Zircon*, 53, p. 469-500.

DePaolo D.J. 1981. Neodymium isotopes in the Colorado Front Range and crust-mantle evolution in the Proterozoic. *Nature*, **291**:193-196.

DePaolo D.J. 1988. *Neodymium isotope geoquemistry – an Introduction*. Springer-Verlag, 490 p.

Eby G.N. 1990. The A-type granitoids: A review of their occurrence and chemical characteristics and speculations on their petrogenesis. *Lithos*, **26**(1-2):115-134.

Eby G.N. 1992. Chemical subdivision of the A-type granitoids: Petrogenetic and tectonic implications. *Geology*, **20**(7):641-644.

Ekren E.B. McIntyre D.H., Bennett E.H. 1984. High-temperature, large-volume, lavalike ash-flow tuffs without calderas in Southwestern Idaho. *Geological Survey Professional Paper 1272*, 1-73.

Elhlou S., Belousova E., Griffin W.L., Pearson N.J., O'Reilly S.Y. 2006. Trace element and isotopic composition of GJ red zircon standard by laser ablation. *Geochimica et Cosmochimica Acta*, **70**:A158.

Fernandes L.A.D., Menegat R., Costa A.F.U., Koester E., Porcher C.C., Tommasi A., Kraemer G., Ramgrab G.E., Camozzato E. 1995. Evolução tectônica do Cinturão Dom Feliciano no Escudo Sul-rio-grandense: Parte I – uma contribuição a partir do registro geológico. *Revista Brasileira de Geociências*, **25**(4):351-374.

Fragoso-César A.R.S., Almeida R.P., Fambrini G.L., Pelosi A.P.M.R., Janikian L. 2003. A Bacia do Camaquã: um sistema intracontinental anorogênico de rifts do Neoproterozóico III, Eopaleozóico no Rio Grande do Sul. *In:* Encontro sobre a estratigrafia do Rio Grande do Sul, 1, *Boletim de Resumos*, Porto Alegre, SBG, v.1, p. 139-144.

Fragoso-César A.R.S., Fambrini G.L., Almeida R.P., Pelosi A.P.M.R., Janikian L., Riccomini C., Machado R., Nogueira A.C.R., Saes G.S. 2000. The Camaquã extensional basin: Neoproterozoic to Early Cambrian sequences in southernmost Brazil. *Revista Brasileira de Geociências*, **30**(3):438-441.

Gastal M.C.P. & Lafon J.M. 1998. Gênese e evolução dos granitóides metaluminosos de afinidade alcalina da porção oeste do escudo sul-riograndense: geoquímica e isótopos de Rb-Sr e Pb-Pb. *Revista Brasileira de Geociências*, **28**(1):11-28.

Gastal M.C.P. & Lafon J.M. 2001. Novas idades 207Pb/ 206Pb e geoquímica isotópica Nd-Sr para granitóides shoshoníticos e alcalinos das regiões de Lavras do Sul e Taquarembó, RS. *In:* VIII Congresso Brasileiro de Geoquímica, 8, Curitiba. *Anais...*,Curitiba, SBGEO, v. 1, p. 21-26.

Gresse P.G., Chemale F., Silva L.C., Walraven F., Hartmann L.A. 1996. Late- to post-orogenic basins of the Pan-African-Brasiliano collision orogen in southern Africa and southern Brazil. *Basin Research*, **8**(2):157-171.

Harris N.B.W., Santosh M., Taylor P.N. 1994. Crustal evolution in south India: constraints from Nd isotopes. *Journal of Geology*, **102**:139–50

Hart S.R. 1988 Heterogeneous mantle domains: signatures, genesis and mixing chronologies. *Earth and Planetary Science Letters*, **90**:273-296.

Hartmann L.A., Chemale Jr. F., Philipp R.P. 2007. Evolução Geotectônica do Rio Grande do Sul no Pré-Cambriano. *In:* Iannuzzi, R. and Frantz, J.C. (eds.) *50 Anos de Geologia. Instituto de Geociências. Contribuições*. Porto Alegre, Comunicação e Identidade, p. 97-123.

Hartmann L.A., Leite J.A.D., McNaughton N.J., Santos J.O.S. 1999. Deepest exposed crust of Brazil-SHRIMP establishes three events. *Geology*, **27**(10):947-950.

Hartmann L.A., Leite J.A.D., Silva L.C., Remus M.V.D., McNaughton N.J., Groves D.I., Fletcher I.R., Santos J.O.S., Vasconcellos M.A.Z. 2000. Advances in SHRIMP geochronology and their impact on understanding the tectonic and metallogenic evolution of southern Brazil. *Australian Journal of Earth Sciences*, **47**(5):829-844.

Janikian L., Almeida R.P., Fragoso-Cesar A.R.S., Corrêa C.R.A., Pelosi A.P.M.R. 2005. Evolução paleoambiental e seqüências deposicionais do Grupo Bom Jardim e da Formação Acampamento Velho (Supergrupo Camaquã) na porção norte da Sub-Bacia Camaquã Ocidental. *Revista Brasileira de Geociências*, **35**(2):245-256.

Janikian L., Almeida R.P., Fragoso-Cesar A.R.S., Martins V.T.S., Dantas E.L., Tohver E., McReath I., D'Agrella-Filho M.S. 2012. Ages (U-Pb SHRIMP and LA ICPMS) and stratigraphic evolution of the Neoproterozoic volcano-sedimentary successions from the extensional Camaquã Basin, Southern Brazil. *Gondwana Research*, **21**(2-3):466-482.

Janikian L., Almeida R.P., Trindade R.I.F., Fragoso-Cesar A.R.S., D'Agrella-Filho M.S., Dantas E.L., Tohver E. 2008. The continental record of Ediacaran volcano-sedimentary successions in southern Brazil and their global implications. *Terra Nova*, **20**(4):259-266.

Le Bas M.J., Le Maitre R.W., Streckeisen A., Zanettin, B. 1986. A chemical classification of volcanic rocks on the total alkali-silica diagram. *Journal of Petrology*, **27**(3):745-750.

Leat P.T., Jackson S.E., Thorpe R.S., Stillman C.J. 1986. Geochemistry of bimodal basalt-subalkaline/peralkaline rhyolite provinces within the Southern British Caledonides. *Journal of the Geological Society*, **143**(2):259-273.

Leitzke F.P., Sommer C.A., Lima E.F., Matté V. 2015. O vulcanismo alta-sílica da região do Tupanci, NW do Escudo Sul-Rio-Grandense: faciologia, petrografia e litoquímica. *Pesquisas em Geociências*, **42**(1):5-24.

Liégeois J.P. 1998. Some words on the post-collisional magmatism. Preface to Special Edition on Post-Collisional Magmatism. ***Lithos***, **45**:15-17.

Lima E.F. & Nardi L.V.S. 1985. Geologia, petrografia e petroquímica das rochas vulcânicas da região de Volta Alegre, Lavras do Sul, RS. *Acta Geologica Leopoldensia*, **20**:15-62.

Lima E.F., Sommer C.A., Nardi L.V.S. 2007. O vulcanismo neoproterozóico-ordoviciano no Escudo Sul-Rio-Grandense: os ciclos vulcânicos da Bacia do Camaquã. *In:* Iannuzzi R. & Frantz J.C. (eds.) *50 Anos de Geologia. Instituto de Geociências. Contribuições*. Porto Alegre, Comunicação e Identidade, p. 79-95.

Logfren G. 1971. Experimentally produced devitrification textures in natural rhyolitic glass. *Geological Society of America Bulletin*, **82**(1):111-124.

Ludwig K.R. 2008. User's manual for Isoplot. *Berkeley Geochronological Center.*

Manley C.R. 1995. How voluminous rhyolite lavas mimic rheomorphic ignimbrites: Eruptive style, emplacement conditions, and formation of tuff-like textures. *Geology*, **23**(4):349-352.

Matté V., Sommer C.A., Lima E.F., Philipp R.P., Basei M.A.S. 2016. Post-collisional Ediacaran volcanism in oriental Ramada Plateau, southern Brazil. *Journal of South American Earth Sciences*, **71**:201-222.

Matté V., Sommer C.A., Lima E.F., Saldanha, D.L., Pinheiro-Sommer J.A., Liz J.D. 2012. Rochas dioríticas do Platô da Ramada, Rio Grande do Sul, e sua relação com o vulcanismo alcalino da Formação Acampamento Velho, Neoproterozoico do Escudo Sul-Rio-Grandense. *Revista Brasileira de Geociências*, **42**(2):343-362.

Menegotto E. & Medeiros E.R. 1976. Contribuição ao estudo das rochas ígneas ácidas da região da Serra Tupanci, RS. *In:* Congresso Brasileiro de Geologia, 29, Ouro Preto. Anais..., Ouro Preto, SBGEO, v. 2, p. 427-432.

Nakamura N. 1974. Determination of REE, Ba, Fe, Mg, Na, and K in carbonaceous and ordinary chondrites. *Geochimica et Cosmochimica Acta*, **38**(5):757-775.

Nardi L. 1991. Caracterização petrográfica e geoquímica dos granitos metaluminosos da associação alcalina: revisão. *Pesquisas em Geociências*, **18**(1):44-57.

Nardi L.V.S. & Bitencourt M.F. 2009. A-type granitic rocks in post-collisional settings in southernmost Brazil: Their classification and relationship with tectonics and magmatic series. *Canadian Mineralogist*, **47**(6):1493-1503.

Nardi L.V.S. & Bonin B. 1991. Post-orogenic and non-orogenic alkaline granite associations: The Saibro intrusive suite, southern Brazil – A case study. *Chemical Geology*, **92**(1-3):197-211.

Nardi L.V.S. & Lima E.F. 2000. O magmatismo Shoshonítico e Alcalino da Bacia do Camaquã - RS. *In:* Holz M. & De Ros L.F. (eds.) *Geologia do Rio Grande do Sul*. Porto Alegre, CIGO/ UFRGS, p. 119-131.

Nardi L.V.S., Plá-Cid J., Bitencourt M.F., Stabel L.Z. 2008. Geochemistry and petrogenesis of post-collisional ultrapotassic syenites and granites from southernmost Brazil: the Piquiri Syenite Massif. *Anais da Academia Brasileira de Ciências*, **80**(2):353-371.

Oliveira D.S., Sommer C.A., Philipp R.P., Lima E.F., Basei M.A.S. 2015. Post-collisional subvolcanic rhyolites associated with the Neoproterozoic Pelotas Batholith, southern Brazil. *Journal of South American Earth Sciences*, **63**:84-100.

Oyhantçabal P., Siegesmund S., Wemmer K. 2011. The Río de la Plata Craton: A review of units, boundaries, ages and isotopic signature. *International Journal of Earth Sciences*, **100**(2-3):201-220.

Paim P.S.G., Chemale Jr. F., Lopes R.C. 2000. A Bacia do Camaquã. *In:* De Ros L.F., Holz M. (eds.) *Geologia do Rio Grande do Sul*. Porto Alegre, CIGO/UFRGS, p. 231-374.

Pearce J.A., Harris N.B.W., Tindle A.G. 1984. Trace element discrimination diagrams for the tectonic interpretation of granitic rocks. *Journal of Petrology*, **25**(4):956-983.

Philipp R. P., Nardi L.V.S., Bitencourt M.F. 2000. O Batólito Pelotas no RS. *In:* Holz M. & De Ros L.F. (eds.) *Geologia do Rio Grande do Sul*. CIGO-UFRGS, Porto Alegre, p. 133-160.

Philipp R.P. & Machado R. 2005. The Late Neoproterozoic granitoid magmatism of the Pelotas Batholith, southern Brazil. *Journal of South American Earth Sciences*, **19**(4):461-478.

Roisenberg A., Formoso M.L., Vieira Jr. N., Dutra C.V., Altamirano J.A.F., Ferreira A.C. 1986. Petrologia e geoquímica do vulcanismo Proterozóico Superior-Eo-paleozóico do Escudo Sul-rio-grandense: Serrinha Tupancí e Cerro dos Lopes. *In:* Congresso Brasileiro de Geologia, 34,Goiânia, GO. Boletim de Resumos..., Goiânia, SBGEO, v. 1. p. 170.

Shellnutt J.G., Wang C.Y., Zhou M-F., Yang Y. 2009. Zircon Lu–Hf isotopic compositions of metaluminous and peralkaline A-type granitic plutons of the Emeishan large igneous province (SW China): Constraints on the mantle source. *Journal of Asian Earth Sciences*, **35**(1):45-55.

Soliani Jr. E., Koester E., Fernandes L.A.D. 2000. A geologia isotópica do Escudo Sul-rio-grandense – Parte I: métodos isotópicos e valor interpretativo. *In:* Holz M. & De Ros L.F. (eds.) *Geologia do Rio Grande do Sul*. CIGO/UFRGS, Porto Alegre, p. 175-230.

Sommer C.A., Lima E.F., Nardi L.V.S. 1999. Evolução do vulcanismo alcalino na porção sul do Platô do Taquarembó, Dom Pedrito, RS. *Revista Brasileira de Geociências*, **29**(2):245-254.

Sommer C.A., Lima E.F., Nardi L.V.S., Figueiredo A.M.G., Pierosan R. 2005a. Potassic and low- and high-Ti mildly alkaline volcanism in the Neoproterozoic Ramada Plateau, southernmost Brazil. *Journal of South American Earth Sciences*, **18**(3-4):237-254.

Sommer C.A., Lima E.F., Nardi L.V.S., Liz J.D., Waichel B.L. 2005b. Neoproterozic, Mildly Alkaline, Bimodal Volcanism in Southern Brazil: Geological and Geochemical Aspects. *International Geology Review*, **47**(10):1090-1110.

Sommer C.A., Lima E.F., Nardi L.V.S., Liz J.D., Waichel B.L. 2006. The evolution of Neoproterozoic magmatism in southernmost Brazil: Shoshonitic, high-K tholeiitic and silica-saturated, sodic alkaline volcanism in post-collisional basins. *Anais da Academia Brasileira de Ciências*, **78**(3):573-589.

Stacey J.S. & Kramers J.D. 1975. Approximation of terrestrial Lead isotope evolution by a 2-stage model. *Earth and Planetary Science Letters*, **26**(2):207-221.

Steiger R.H. & Jäger E. 1977. Subcommission on Geochronology: Convention on the use of decay constants in geo- and cosmochronology. *Earth and Planetary Science Letters*, **36**(3):359-362.

Teixeira A.L., Gaucher C., Paim P.S.G., Fonseca M.M., Parente C.V., Silva Vilho W.F., Almeida A.R. 2004. Bacias do Estágio de transição da Plataforma Sul-Americana. *In:* Mantesso-Neto V., Bartorelli A., Carneiro C.D.R., Brito Neves B. (eds.) *Geologia do continente Sul-Americano*. São Paulo, p. 487-537.

Tera F. & Wasserburg G.J. 1972. U–Th–Pb systematics in lunar highland samples from the Luna 20 and Apollo 16 missions. *Earth and Planetary Science Letters*, **17**(1):36-51.

Verma S.P., Torres-Alvarado I.S., Satir M., Dobson P.F. 2005. Hydrotermal alteration effects in geochemistry and Sr, Nd, Pd and O isotopes of magmas from the Los Azufres geothermal field (Mexico): A statistical approach. *Geochemical Journal*, **39**(2):141-163.

Wasserburg G.J., Jacobsen S.B., De Paolo D.J., McCulloch M.T., Wen T. 1981. Precise determination of Sm/Nd ratios, Sm and Nd isotopic abundances in standard solutions. *Geochimica et Cosmochimica Acta*, **45**(12):2311-2323.

Wetherill G.W. 1957. 1956. Discordant Uranium-Lead Ages, I. *Transactions, American Geophysical Union*, **37**(3): 320-326.

Whalen J.B., Currie K.L., Chappell B.W. 1987. A-type granites: Geochemical characteristics, discrimination and petrogenesis. *Contributions to Mineralogy and Petrology*, **95**(4):407-419.

Wildner W., Lima E.F., Nardi L.V.S., Sommer C.A. 2002. Volcanic cycles and setting in the Neoproterozoic III to Ordovician Camaquã Basin succession in southern Brazil: Characteristics of post-collisional magmatism. *Journal of Volcanology and Geothermal Research*, **118**(1-2):261-283.

Wildner W., Nardi L.V.S., Lima E.F. 1999. Post-collisional Alkaline Magmatism on the Taquarembó Plateau: A well-preserved Neoproterozoic-Cambrian Plutono-volcanic Assocition in Southern Brazil. *International Geology Review*, **41**(12):1082-1098.

Winchester J.A. & Floyd P.A. 1977. Geochemical discrimination of different magma series and their differentiation products using immobile elements. *Chemical Geology*, **20**:325-343.

Available at www.sbgeo.org.br